Sufficient Conditions for Robust Frequency Stability of AC Power Systems

Erick Alves [ID], *Senior Member, IEEE*, Gilbert Bergna-Diaz [ID], *Member, IEEE*, Danilo Brandao [ID], *Member, IEEE*, and Elisabetta Tedeschi [ID], *Senior Member, IEEE*

Abstract—**This paper analyses the frequency stability of ac grids in the presence of non-dispatchable generation and stochastic loads. Its main goal is to evaluate conditions in which the system is robust to large, persistent active power disturbances without recurring to time-domain simulations. Considering the ongoing energy transition to more renewable sources, defining robustness boundaries is a key topic for power system planning and operation. However, much of the research on long-term studies has not dealt with robust dynamic constraints, while short-term analyses usually depend on time-consuming simulations to evaluate nonlinearities. To bridge this gap, the authors derive an algebraic equation that provides sufficient conditions for robust frequency stability in ac power systems and a relationship among four key quantities: the maximum active power perturbation, the minimum system damping, the steady-state and the transient frequency limits. To achieve this goal, it uses a nonlinear average-model of the ac grid and Lyapunov's direct method extended by perturbation analysis requiring only limited knowledge of the system parameters. The algebraic calculations are validated using time-domain simulations of the IEEE 39-bus test system and results are compared to the traditional Swing Equation model.**

Index Terms—**Power system dynamics, power system planning, power system simulation, power system stability, robustness, frequency stability, Lyapunov methods.**

I. INTRODUCTION

ANY modern society requires an energy system that is affordable, accessible, secure and sustainable. However, recent technological advancements and social changes have been challenging the limits of this balance and pushing for a complete rethinking of energy systems. Electric power generation is now: 1) becoming more decentralized; 2) taking place closer to final users; 3) undergoing a technological transformation that comprehends more diversified primary sources, new forms of energy storage and power electronics [1], [2].

In this new paradigm, planning and operation of electrical ac grids are becoming more involved. For instance, conversion from primary sources and storage is performed using not only synchronous machines but also converter-interfaced generators (CIGs). The latter can supply up to 50% of the annual demand and 100% of the hourly demand in places such as Colorado, Denmark, Hawaii, Ireland, Tasmania, Texas and South Australia [3], [4]. This introduces new dynamics into the electric power system that are "yet to be fully understood" [5] and blurry the boundaries to which well-established models can be applied [6].

Moreover, groups of interconnected loads and distributed energy resources, also known as microgrids (MGs) [7], [8], can form islands and operate independently from the bulk power system. However, this desired feature is only achieved when primary sources, storage units, power converters and control systems are properly planned, designed and operated.

From this perspective, one of the main challenges is defining sufficient conditions for stable operation of low-inertia systems in islanded mode [2]. Stability here is seen in the sense of system states remaining within acceptable ranges for given changes in inputs, i.e. input-to-state stability. In recent years, this topic has been an active area of research and references [5], [9] present extensive reviews on it. Providing proper models and clear stability criteria is essential for tasks, such as: 1) setting proper controller gains [10], [11]; 2) establishing technical constraints for dispatching [12]; 3) deciding about load shedding or generation curtailment [13].

Specifically, guaranteeing frequency stability of low-inertia systems can be a major challenge and requires proper sizing of dispatchable power sources and energy storage. Nevertheless, an inspection of recent literature reviews on ac MG planning [14], [15] shows that conditions for frequency stability are largely overlooked in the problem formulation. Specifically, most optimization algorithms assume that matching power demand with production is the only required dynamic constraint, without imposing minimum requirements on system damping or frequency containment reserves (FCR). While such results may be optimal from the affordability point of view, they could be questionable from the security aspect and may be operationally unfeasible.

On the other hand, an inspection of the literature reveals that methods for designing low-inertia power systems in the presence of stochastic loads and non-dispatchable generation

Erick Alves and Gilbert Bergna-Diaz are with the Department of Electric Power Engineering, Norwegian University of Science and Technology, 7034 Trondheim, Norway (e-mail: erick.f.alves@ntnu.no; gilbert.bergna@ntnu.no).

Elisabetta Tedeschi is with the Department of Electric Power Engineering, Norwegian University of Science and Technology, 7034 Trondheim, Norway, and also with the Department of Industrial Engineering, University of Trento, 38123 Trento, Italy (e-mail: elisabetta.tedeschi@ntnu.no).

Danilo Brandao is with the Graduate Program in Electrical Engineering, Federal University of Minas Gerais, Belo Horizonte, 30150-311, Brazil (e-mail: daniloiglesiasb@yahoo.com.br).

Color versions of one or more figures available at https://doi.org/10.1109/TPWRS.2020.3039832.

Digital Object Identifier 10.1109/TPWRS.2020.3039832

considering frequency stability constraints have been proposed lately. Some time ago, [16] introduced a method to optimally size and operate an energy storage system that provides FCR in an isolated power system (IPS) with wind, hydraulic, gas turbines and stochastic loads. Results were validated using a dynamic model in Matlab Simulink. In addition, [17] demonstrated how a fast-acting energy storage can increase the frequency stability of the Guadaloupe archipelago in the Caribbean and reduce the actuation of automatic load shedding using power-hardware-in-the-loop simulations. In [18], the authors also used time-domain simulations (TDSs) to study how the size and controller settings of an energy storage based on ultracapacitors impacted the frequency stability and the performance of the automatic load shedding scheme in the IPS of La Palma, Spain. Later, the same authors extended this work with field-tests results in [19]. Not least, [20] solved the unit commitment problem including FCR constraints for an IPS using mixed-integer linear programming. For that, it determined the minimum system damping empirically relying on the load-frequency sensitivity index. Moreover, frequency stability constraints have been proposed in planning and operation studies, such as optimal power flow problems [21]–[24].

Note that, in the different approaches discussed above, there is a heavy reliance on TDSs and/or model linearization to establish key boundaries for frequency stability. TDSs provide the most accurate results but are hard to integrate in optimization problems such as optimum power flow, while linearizations around an operation point do not give realistic values for frequency deviations during large active power disturbances (APDs). Taking into account this background, the main contribution of this paper is the derivation of sufficient conditions for frequency stability of an ac power system where sources and loads are subject to non-vanishing, bounded perturbations. Using a nonlinear average-model of the ac grid, Lyapunov's direct method and perturbation analysis, an algebraic equation is derived and provides a relationship among four boundaries: the maximum APD, the minimum system damping, the steady-state and the transient frequency limits. The main goal is providing a framework to implement frequency stability constraints in optimization algorithms without recurring to time-consuming simulations or unnecessary linearizations of the power balance equations.

The text is organized as follows: section II introduces a nonlinear, average model of the ac grid that is appropriate for frequency stability analysis during large APDs; section III presents the main proposition of this work followed by its mathematical proof; section IV validates the proposition using time-domain simulations of the IEEE 39-bus test system [26] and compares its results to the linear Swing Equation model; section V discusses applications of the proposition, its main limitations and directions for future research; finally, section VI presents the concluding remarks.

II. Nonlinear Average Model of an AC Power System

When omitting network topology and voltage dynamics, the average behavior of an ac grid angular speed can be modeled using first principles as an equivalent rotating mass using Newton's second law of motion [5], [26]:

$$J\dot{\omega} = T_S(t,\omega) - T_L(t,\omega) - B(t)(\omega - \omega_s) \tag{1}$$

where J is the equivalent moment of inertia [kgm^{-2}] of the system and $B(t)$ is a time-varying function representing the equivalent damping coefficient [Nmsrad^{-1}] of the system; $T_S(t,\omega)$ and $T_L(t,\omega)$ are the equivalent torques from sources and loads [Nm], functions of the time t [s] and the center of inertia (COI) angular speed ω [rads^{-1}]; ω_s is a constant representing the synchronous angular speed [rads^{-1}].

Proposition 1: The nonlinear system in eq. (1) can be expressed as:

$$\dot{\widetilde{x}} = f(t,\widetilde{x}) + g(t,\widetilde{x})$$

where $\widetilde{x}$ is the state variable of the system, $f(t,\widetilde{x})$ is piecewise continuous in t and represents the dynamics of the system, $g(t,\widetilde{x})$ is a perturbation term that results from uncertainties and disturbances.

Proof: Eq.(1) can be rearranged into the desired form when multiplying it by ω and normalizing it with the system base power (S_b) [W]:

$$\omega J\dot{\omega} = \omega T_S(t,\omega) - \omega T_L(t,\omega) - \omega B(t)(\omega - \omega_s)$$

$$= P_S(t,\omega) - P_L(t,\omega) - \omega B(t)(\omega - \omega_s)$$

$$\frac{\omega J}{S_b}\dot{\omega} = \frac{P_S(t,\omega)}{S_b} - \frac{P_L(t,\omega)}{S_b} - \omega\frac{B(t)(\omega - \omega_s)}{S_b}$$

$$xM\dot{x} = u(t,x) - w(t,x) - xD(t)(x-1)$$

$$\dot{x} = -\frac{D(t)}{M}(x-1) + \frac{u(t,x) - w(t,x)}{xM}$$

$$\dot{\widetilde{x}} = \underbrace{-\frac{D(t)}{M}\widetilde{x}}_{f(t,\widetilde{x})} + \underbrace{\frac{u(t,\widetilde{x}) - w(t,\widetilde{x})}{(\widetilde{x}+1)M}}_{g(t,\widetilde{x})} \tag{2}$$

where $x = \frac{\omega}{\omega_s}$ and $\widetilde{x} = x - 1$ are the normalized COI angular speed and the COI angular speed deviation from the synchronous speed [pu]; $M = \frac{J\omega_s^2}{S_b}$ and $D(t) = \frac{B(t)\omega_s^2}{S_b}$ are the normalized equivalent moment of inertia [s] and damping coefficient [pu]; $P_S(t,\omega)$ and $P_L(t,\omega)$ are the total active power from sources and loads [W]; $u(t,\widetilde{x})$ and $w(t,\widetilde{x})$ are the normalized total active power from sources and loads [pu]. ∎

III. Sufficient Conditions for Robust Frequency Stability

This section introduces the main proposition of this paper, which is an algebraic expression relating four key boundaries in an ac power system: the maximum APD $\|u(t,\widetilde{x}) - w(t,\widetilde{x})\| < P_b$ [pu], the minimum system damping $D_{\min}$ [pu], the steady-state r_{ss} and the transient r_{tr} frequency limits [pu]. Once three of these boundaries are set, the fourth can be unequivocally defined. While the involved mathematical proof of this proposition is presented in detail below, there will be no loss of understanding by proceeding directly to eq. (4), which summarizes the relationship between these quantities.

Proposition 2: Let $\|u(t,\widetilde{x}) - w(t,\widetilde{x})\| < P_b$ be the maximum APD of the system defined in eq. (2) in which M is a positive constant, $D(t)$ is piecewise continuous in the time t and lower-bounded by a positive constant $D_{\min}$.

If $\quad P_b = D_{\min}r_{ss}(1 - r_{tr})$, $\forall t \geq 0$, $\widetilde{x} \in \mathbb{D} = \{\widetilde{x} \in \mathbb{R} \mid \|\widetilde{x}\| \leq r_{tr}, 0 < r_{tr} < 1\}$ where r_{tr}, r_{ss} are the maximum allowed values of $\widetilde{x}$ during the transient and steady-state periods, respectively.

Then, for all $\|\widetilde{x}(t_0)\| < r_{ss}$ and $r_{ss} < r_{tr}$, the solution $\widetilde{x}$ of eq. (2) satisfies

$$\|\widetilde{x}\| \leq exp[-\gamma(t - t_0)]r_{tr}, \; t_0 \leq t < t_0 + T$$

$$\|\widetilde{x}\| \leq r_{ss}, \; \forall t \geq t_0 + T$$

for $\gamma = (1 - \frac{r_{ss}}{r_{tr}})\frac{D_{\min}}{M}$ and some finite T that represents the duration of the transient period.

Proof: Let $\mathcal{V}(\widetilde{x}) = \frac{M}{2}\widetilde{x}^2$ be an input-to-state Lyapunov function candidate for the system in eq. (2). Note that $\mathcal{V}(\widetilde{x})$ is: 1) a piecewise, continuous differentiable function on $\mathbb{R}$; 2) class $\mathcal{K}_\infty$ according to definition 4.2 in [27]; 3) upper- and lower-bounded by $\frac{M}{2}\|\widetilde{x}\|^2$. Moreover, its time derivative is given by:

$$\dot{\mathcal{V}}(t,\widetilde{x}) = \widetilde{x}^\top M\dot{\widetilde{x}}$$

$$= -D(t)\widetilde{x}^2 + \frac{\widetilde{x}}{\widetilde{x} + 1}(u(t,\widetilde{x}) - w(t,\widetilde{x})) \quad (3)$$

Assuming that $\widetilde{x} \in \mathbb{D}$ and using the Cauchy-Schwarz's inequality, it holds that:

$$\dot{\mathcal{V}}(t,\widetilde{x}) \leq -D_{\min}\|\widetilde{x}\|^2 + \frac{\|\widetilde{x}\|}{1 - r_{tr}}(\|u(t,\widetilde{x}) - w(t,\widetilde{x})\|)$$

$$\leq -D_{\min}(1 - \theta)\|\widetilde{x}\|^2$$

$$- \|\widetilde{x}\|\left(D_{\min}\theta\|\widetilde{x}\| - \frac{\|u(t,\widetilde{x}) - w(t,\widetilde{x})\|}{1 - r_{tr}}\right)$$

$$\leq -W_3(\widetilde{x}), \; \forall\|\widetilde{x}\| \geq \rho(\|u(t,\widetilde{x}) - w(t,\widetilde{x})\|) > 0$$

where $0 < \theta < 1$, $D_{\min} > 0$, $W_3(\widetilde{x}) = D_{\min}(1 - \theta)\|\widetilde{x}\|^2$ and $\rho(\|z\|) = \frac{\|z\|}{(1 - r_{tr})D_{\min}\theta}$.

As $W_3(\widetilde{x})$ is a continuous positive definite function on $\mathbb{R}$ and $\rho(\|z\|)$ is class $\mathcal{K}$, all conditions of the input-to-state theorem in Appendix C are fulfilled. Hence, the system defined in eq. (2) is input-to-state stable on $\mathbb{D}$.

Now, let us analyze the unforced system, i.e. the case where $\|u(t,\widetilde{x}) - w(t,\widetilde{x})\| = 0$. The inequalities:

$$c_1\|\widetilde{x}\|^2 \leq \mathcal{V}(t,\widetilde{x}) \leq c_2\|\widetilde{x}\|^2$$

$$\dot{\mathcal{V}}(t,\widetilde{x}) \leq -c_3\|\widetilde{x}\|^2$$

$$\left\|\frac{\delta\mathcal{V}}{\delta\widetilde{x}}\right\| \leq c_4\|\widetilde{x}\|$$

are derived directly from eq. (3) and the assumptions in Proposion 2 where $c_1 = c_2 = \frac{M}{2}$, $c_3 = D_{\min}, c_4 = M$ are positive constants. These are valid for all $(t, x) \in [0, \infty) \times \mathbb{D}$. Consequently, the unforced system fulfills all conditions from Theorem 4.10 in [27] and $\widetilde{x} = 0$ is exponentially stable on $\mathbb{D}$.

With the previous results, it is possible to apply lemma 9.2 in [27]. In this context, when assuming that:

1) $g(t,\widetilde{x}) = \dfrac{u(t,\widetilde{x}) - w(t,\widetilde{x})}{(\widetilde{x} + 1)M}$ is the perturbation term of the system in eq. (2)

2) $\|\widetilde{x}(t)\|$ must be bounded by r_{ss}, i.e. $b = \frac{c_4}{c_3}\sqrt{\frac{c_2}{c_1}}\frac{\delta}{\theta} = r_{ss}$

3) $r_{ss} = r_{tr}\theta$

it follows that:

$$\|g(t,\widetilde{x})\| \leq \delta < \frac{c_3}{c_4}\sqrt{\frac{c_1}{c_2}}r_{tr}\theta$$

$$\left\|\frac{u(t,\widetilde{x}) - w(t,\widetilde{x})}{M(\widetilde{x} + 1)}\right\| < \frac{D_{\min}}{M}r_{tr}\theta$$

$$\frac{\|u(t,\widetilde{x}) - w(t,\widetilde{x})\|}{M\|\widetilde{x} + 1\|} < \frac{D_{\min}}{M}r_{ss}$$

$$\|u(t,\widetilde{x}) - w(t,\widetilde{x})\| < \underbrace{D_{\min}r_{ss}(1 - r_{tr})}_{P_b}$$

for all $t \geq 0$, all $\widetilde{x} \in \mathbb{D}$ and $0 < r_{ss} < r_{tr}$.

Hence, if the maximum APD satisfies the upper-bound:

$$P_b = D_{\min}r_{ss}(1 - r_{tr}) \quad (4)$$

Then, for all $\|\widetilde{x}(t_0)\| < r_{ss}$ and for some finite T, the solution $\widetilde{x}(t)$ of eq. (2) satisfies:

$$\|\widetilde{x}\| \leq exp[-\gamma(t - t_0)]r_{tr}, \; t_0 \leq t < t_0 + T$$

$$\|\widetilde{x}\| \leq r_{ss}, \; \forall t \geq t_0 + T$$

where the minimum convergence rate of $\|\widetilde{x}\|$ is:

$$\gamma = \left(1 - \frac{r_{ss}}{r_{tr}}\right)\frac{D_{\min}}{M} \quad (5)$$

In summary, the steps of the proof are the following:
1) Show that the system in eq. (2) is input-to-state stable on $\mathbb{D}$ using the input-to-state theorem in Appendix C.
   - Use $\mathcal{V}(\widetilde{x}) = \frac{M}{2}\widetilde{x}^2$ as Lyapunov function candidate.
   - Use the Cauchy-Schwarz's inequality to show that $\frac{1}{\|\widetilde{x}+1\|} \leq \frac{1}{1 - r_{tr}}$ when $\widetilde{x} \in \mathbb{D}$.
2) Using Theorem 4.10 in [27], show that $\widetilde{x} = 0$ is an exponentially stable equilibrium point of the unforced system, i.e. $g(t,\widetilde{x}) = 0$ in eq. (2).
3) Apply Lemma 9.2 in [27] assuming that:
   - $g(t,\widetilde{x}) = \frac{u(t,\widetilde{x}) - w(t,\widetilde{x})}{(\widetilde{x}+1)M}$ is the perturbation term of the system in eq. (2)
   - The state must be bounded by r_{ss}, i.e. $b = \frac{c_4}{c_3}\sqrt{\frac{c_2}{c_1}}\frac{\delta}{\theta} = r_{ss}$
   - $r_{ss} = r_{tr}\theta$ ∎

Remark 2.1: The time intervals from Proposion 2 can be divided in:
- $t < t_0$ is the steady-state period before the APD $\|u(t,\widetilde{x}) - w(t,\widetilde{x})\| < P_b$ appears at $t = t_0$. The system is in an equilibrium point $\widetilde{x}(t_0)$ whose norm is upper-bounded by r_{ss}.
- $t_0 \leq t < t_0 + T$ is the transient period after the APD is applied to the system at $t = t_0$ in which the state norm $\|\widetilde{x}(t)\|$ is upper-bounded by $exp[-\gamma(t - t_0)]r_{tr}$, where

$\gamma = (1 - \frac{r_{ss}}{r_{tr}})\frac{D_{\min}}{M}$ is the minimum convergence rate from $\widetilde{x}(t_0)$ to $\widetilde{x}(t_0 + T)$.

- $t \geq t_0 + T$ is the steady-state period after the system settles down on the new equilibrium point $\widetilde{x}(t_0 + T)$, whose norm is upper-bounded by r_{ss}.

Remark 2.2: The proof assumes that $\widetilde{x}$ always remains in $\mathbb{D}$. In other words, Proposition 2 is only valid when $\widetilde{x}$ lies between $-r_{tr}$ and r_{tr}. Though, note that this is a reasonable assumption. In ac power systems, when $\widetilde{x} \notin \mathbb{D}$, load shedding or generation curtailment will take place to reduce the power imbalance and bring it back to $\mathbb{D}$.

Remark 2.3: The inequality $\frac{1}{\|\widetilde{x}+1\|} \leq \frac{1}{1-r_{tr}}$ and, hence, Proposition 2 are valid when $0 < r_{tr} < 1$, i.e. $0 < \omega < 2\omega_s$. For most ac power systems, this is a reasonable assumption.

Remark 2.4: As seen in eq. (5), γ and hence the maximum rate of change of frequency (RoCoF) is dependent on $D_{\min}$ and M. However, the equilibrium point of the system is independent of M, as highlighted in eq. (4). This statement is formally justified with an equilibrium analysis in Appendix A.

Remark 2.5: From a practical perspective, $\theta = \frac{r_{ss}}{r_{tr}}$ is a safety margin. The closer to 1 its value is, the closer to marginal stability the system will be after an APD of amplitude P_b. When ignoring the term $(1 - r_{tr})$, eq. (4) reduces to $P_b = D_{\min}r_{ss}$ which is the expression retrieved from the linear Swing Equation [28], [29].

Remark 2.6: In the problem formulation, time delays in actuators of primary frequency controllers are neglected. While they affect the dynamics of the system and important benchmarks such as the RoCoF, the frequency nadir and zenith, time delays have no influence in the new equilibrium point of the system after a large APD. Appendix B formally justifies this statement.

IV. VALIDATION USING THE IEEE 39-BUS TEST SYSTEM

At first, the advantages of the proposed model over the linear Swing Equation model may not be obvious. Therefore, this section presents study cases of large APDs in the IEEE 39-bus test system [25]. The aim is to compare results of rms TDSs in DIgSILENT PowerFactory 2020 SP2 with algebraic calculations using eq. (4) and the reference equation $P_b = D_{\min}r_{ss}$ derived from the linear Swing Equation model.

Fig. 1 shows the single-line diagram of the IEEE 39-bus test system and Table I and II introduce relevant system parameters used in the calculations. For all simulations and calculations presented herein, $S_b = 100$ MW. Further details required to reproduce the results in this section are available in [30], which contains the model file and its thorough documentation including a description of modeling differences when compared to [25].

A. Load Damping

The damping coefficient D introduced in eq. (2) can be subdivided into:

$$D = D_L + \sum_i D_i \qquad (6)$$

where D_L is the load damping and $\sum_i D_i$ is the sum of frequency droop of all primary frequency controllers. In real
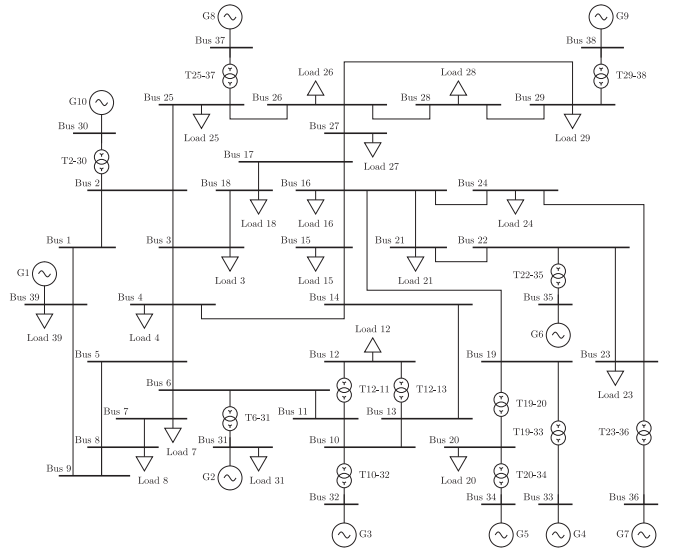

Fig. 1. Single-line diagram of the IEEE 39-bus test system.

TABLE I
INITIAL CONDITIONS OF THE STUDY-CASE

Load	Demand [MW]	Gen.	Injection [MW]	Up-regulation capacity [MW]
3	322	1	1000	0
4	500	(slack) 2	520.8	74.2
7	233.8	3	650	30
8	522	4	632	48
12	7.5	5	508	2
15	320	6	650	30
16	329	7	560	35
18	158	8	540	55
20	628	9	830	20
21	274	10	250	600
23	247.5	Σ	6140.8	894.2
24	308.6			
25	224			
26	139			
27	281			
28	206			
29	283.5			
31	9.2			
39	1104			
Σ	6097.1			

systems, D_L is typically defined either introducing APDs or applying statistical methods such as system identification to historical data [20].

For the study case, the term $\sum_i D_i = 471.75$ is directly retrieved from Table II. However, for the initial conditions shown in Table I, the up-regulation capacity of $G5$ is extremely limited and this unit will saturate for very small net-load increases. Therefore, its damping is ignored, i.e. $\sum_i D_i = 446.25$, and $G5$ is considered a constant active power source at rated capacity during a net-load increase. To maintain the energy balance, the

TABLE II
RELEVANT DATA OF EACH GENERATOR AND ITS PRIMARY FREQUENCY
CONTROLLER WHEN $S_b = 100$ MW

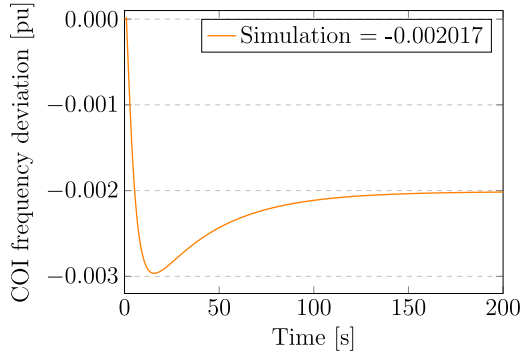| Gen.	Rated active power [MW]	D [pu] (gen. base)	D [pu] (sys. base)	M [s] (sys. base)
1	1000	0	0	500.0
2	595	5	29.75	30.3
3	680	5	34	35.8
4	680	5	34	28.6
5	510	5	25.5	26.0
6	680	5	34	34.8
7	595	5	29.75	26.4
8	595	5	29.75	24.3
9	850	5	42.5	34.5
10	850	25	212.5	42.0
Σ			471.75	782.7

Fig. 2.   COI frequency after increasing bus 4 load by 100 MW.

up-regulation capacity of $G5$ is subtracted from the APD for all calculations.

With the assumptions above, D_L is obtained by suddenly increasing bus 4 load by 100 MW (20% step) and analyzing the load-frequency sensitivity index. Fig. 2 shows the COI frequency deviation of the TDSs in PowerFactory and a new equilibrium at -0.002017 pu. Substituting its absolute value as r_{ss} in the linear and eq. (4) models, assuming that $r_{ss} = r_{tr}$ (i.e. no safety margin) and $P_b = \frac{100-2}{100} = 0.98$ pu:

$$D_L^l = \frac{P_b}{r_{ss}} - \sum_i D_i$$

$$= \frac{0.98}{0.002017} - (446.25) = 39.62$$

$$D_L^p = \frac{P_b}{r_{ss}(1 - r_{tr})} - \sum_i D_i$$

$$= \frac{0.98}{0.002017(1 - 0.002017)} - (446.25) = 40.60$$

where D_L^l is the load damping calculated using the linear model and D_L^p using eq. (4). Note that D_L^p is almost 2.5% higher than D_L^l.
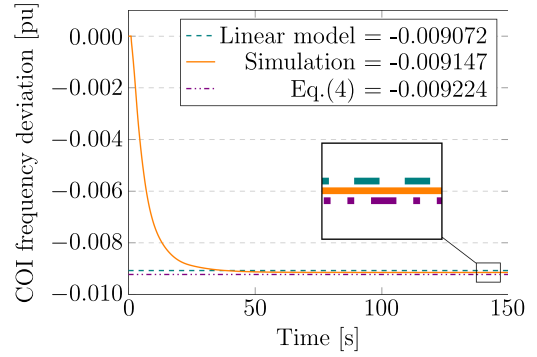

Fig. 3.   COI frequency after the outage of generator 10.

B. Generator 10 Outage

Next, let us compare the results of TDSs with the linear Swing Equation and proposed models for an outage of $G10$, which is a hydro unit providing most of the FCR. For that, let assume that $r_{tr} = 0.02$ pu, which is the value for maximum instantaneous frequency deviation allowed in the Nordic system, as defined in article 127 and annex III of the European grid code [31]. The latter also imposes a maximum steady-state frequency deviation of 0.01 pu, which will be considered the target for r_{ss}.

Under these assumptions, let us consider that $G10$'s initial injection of 250 MW and damping of 212.5 pu are lost. Hence, $P_b = \frac{250-2}{100} = 2.48$ pu and $\sum_i D_i = 446.25 - 212.5 = 233.75$. Substituting in the linear and eq. (4) models:

$$r_{ss}^l = \frac{P_b}{(D_L + \sum_i D_i)}$$

$$= \frac{2.48}{39.62 + 233.75} = 0.009072$$

$$r_{ss}^p = \frac{P_b}{(D_L + \sum_i D_i)(1 - r_{tr})}$$

$$= \frac{2.48}{(40.60 + 233.75)(1 - 0.02)} = 0.009224$$

where r_{ss}^l is the steady-state frequency calculated using the linear model and r_{ss}^p using eq. (4). Fig. 3 compares the two calculated limits with the TDSs and shows that the linear Swing Equation model gives optimistic results which are 0.82% below the TDS's new equilibrium at -0.009147 pu. On the other hand, eq. (4) model provides pessimistic results which are 0.84% above the new equilibrium. Regardless, the three obtained references are below the adopted target for r_{ss} and the test system can robustly operate for net-load variations of up to 250 MW without $G10$.

C. Islanding

In this TDS, the test system is islanded from the bulk grid by disconnecting $G1$. As before, results are compared to the proposed and linear models.

Under the same assumptions from section IV-B, consider that $G1$'s initial injection is lost. Note that no damping is provided by the interconnection. Thus, $\sum_i D_i = 446.25$ and $P_b = \frac{1000-2}{100} =$
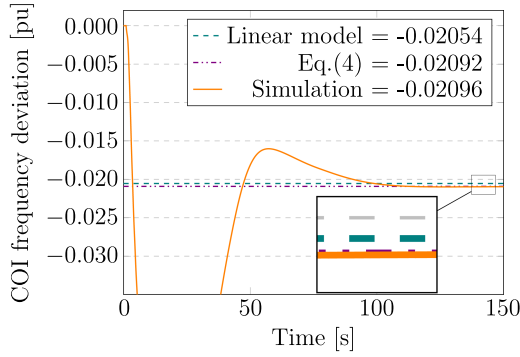
Fig. 4. COI frequency after the system is islanded.

9.98 pu. Substituting in the linear and eq. (4) models:

$$r_{ss}^l = \frac{P_b}{(D_L + \sum_i D_i)}$$
$$= \frac{9.98}{39.62 + 446.25} = 0.02054$$
$$r_{ss}^p = \frac{P_b}{(D_L + \sum_i D_i)(1 - r_{tr})}$$
$$= \frac{9.98}{(40.60 + 446.25)(1 - 0.02)} = 0.02092$$

Fig. 4 compares the two calculated limits with the TDSs and shows that the linear model gives optimistic values which are 2% below the TDS's new equilibrium at -0.02096, while the proposed model provides optimistic values which are 0.2% below the TDSs result. Though, eq. (4) discrepancy occurs because $r_{ss} > r_{tr}$, which invalidates the assumptions from Proposion 2. This indicates that additional measures for frequency stability are required, such as reducing the initial injection of $G1$ or increasing FCR. The reader is invited to recalculate r_{ss}^p using r_{tr} larger than the new equilibrium to confirm that the proposed model will produce pessimistic values as long as $r_{ss} < r_{tr}$.

Note that a recalculation of D or P_b using the linear model does not guarantee frequency stability, as it produces optimistic values. On the contrary, eq. (4) produces pessimistic values whenever $r_{ss} < r_{tr}$ and provides a stability certificate against the nonlinearities introduced in eq. (2).

V. Discussion

At this point, the utility of Proposion 2 may be more apparent. By deriving sufficient conditions for robust frequency stability of ac power systems operating under large APDs, it defines an algebraic relationship between four system boundaries: the maximum APD P_b, the minimum equivalent damping coefficient $D_{\min}$, the transient r_{tr} and r_{ss} steady-state frequency limits. This relationship is summarized in eq. (4) and allows calculation of one of these boundaries once the other three are predefined without resorting to time-consuming TDSs.

As shown in section IV, the proposed algebraic equation produces more realistic forecasts of the COI frequency deviation under large APDs than the linear Swing Equation model. The proposed boundary is robust to nonlinearities and includes

a safety factor that depends on the relationship between the maximum instantaneous and steady-state frequency deviations allowed by grid codes or industry standards. One may argue that deviations corrected by eq. (4) are minimal in large ac grids, where frequency deviations and nonlinearities are minimal. Though, that might not be the case in low-inertia systems, where frequency excursions could be considerable under large APDs. Therefore, the use of eq. (4) may be preferred when an algebraic equation must evaluate the frequency stability of generalized ac grids. Note the model described in section II and the theory applied in section III can be used to study frequency stability of MGs dominated by CIGs if primary controllers use droop control or equivalent strategies [32].

Naturally, TDSs still provide the most accurate results and include assessment of voltage and rotor angle stability, which are ignored in the proposed model. However, the algebraic expression given in eq. (4) allows easy integration of frequency stability criteria in long-term optimization algorithms, such as sizing of primary sources and energy storage, uncertain unit commitment and economic dispatch. For instance, some of the authors are contributing to the project HES-OFF [33] in which a software tool is being developed to reduce greenhouse gases emissions of offshore oil and gas installations by integrating a wind farm and hydrogen-based energy storage in their power generation systems. In HES-OFF, eq. (4) is integrated into a multi-objective, long-term optimization procedure that considers frequency stability criteria in the design stage of the ac power system. The procedure is described in detail in [34], [35]. The proposed model reduced the total optimization time by one order of magnitude when compared to the algorithm recurring to TDSs.

Once again, it is important to emphasize that while criteria offered by Proposion 2 are sufficient from a frequency stability perspective, they are only required conditions for the overall stability of an ac power system. The model developed in section II ignores network topology and voltage dynamics, therefore rotor angle and voltage stability criteria are not considered. Evidently, analysis of these dynamics requires detailed models of synchronous machines and CIGs, as described in [36]. To make the problem more tractable, it might be interesting to apply the standard singular perturbation model described in [27] and divide the analysis in two time scales: slow (frequency) and fast (rotor angle and voltage) dynamics. This approach is one possible direction for future research.

Another limitation of this work is assuming that r_{tr} is not violated. As commented in remark 2.6, time delays of primary frequency controllers influence the RoCoF, the frequency nadir and zenith. In low-inertia systems, this might require the reduction of controller delays, as discussed in Appendix B. On one hand, the time-delay of FCR is a variable that typically cannot be influenced. On the other hand, this scenario is changing by the introduction of fast frequency reserves (FFR). For instance, in the Nordic synchronous areas, market solutions for the procurement of FFR have been recently introduced [37], [38]. Consequently, how to optimally size FFR and FCR simultaneously to achieve frequency stability at a limit r_{ss} without infringing a limit r_{tr} during transients is another interesting topic for future

research, in which the framing presented in this paper might be useful.

VI. CONCLUSION

Using Lyanpunov's direct method extended by perturbation theory, this article proposed sufficient conditions for frequency stability in ac power systems in the presence of active power disturbances originated by non-dispatchable sources and stochastic loads. By doing that, it defined a clear relationship between four system boundaries: the maximum active power disturbance, the minimum equivalent damping coefficient, the transient and steady-state frequency limits. Hence, when three of these boundaries are defined, the fourth is obtained without recurring to time-consuming simulations. The latter feature allows its integration into long-term optimization algorithms such as: sizing of primary sources and energy storage, uncertain unit commitment and economic dispatch. The proposition is validated using time-domain simulations of the IEEE 39-bus test system and compared to the results of the linear Swing Equation model. Moreover, limitations and possible directions for future research are also discussed.

APPENDIX A
EQUILIBRIUM ANALYSIS

Let us define the admissible equilibrium set of the system in eq. (2) as

$$\mathcal{E} \triangleq \left\{ \widetilde{x} \in \mathbb{D} \mid 0 = -\frac{D}{M}\widetilde{x} + \frac{u-w}{(\widetilde{x}+1)M} \right\}$$

Solving in $x^\star, u^\star, w^\star$:

$$\frac{D}{M}x^\star = \frac{u^\star - w^\star}{(x^\star + 1)M}$$

$$x^{\star 2} + x^\star - \left(\frac{u^\star - w^\star}{D} \right) = 0$$

$$x^\star = -\frac{1}{2} \pm \sqrt{\frac{1}{4} + \left(\frac{u^\star - w^\star}{D} \right)} \qquad (7)$$

Note that if $u^\star = w^\star$ (i.e. no active power imbalance), eq. (7) has two solutions: $x^\star = 0$ and $x^\star = -1$. The latter is not in $\mathbb{D}$, so only the former is valid. In conclusion, the equilibrium around $x^\star = 0$ is independent of M and affected only by D and $u^\star - w^\star$, as highlighted in eq. (4) and (7).

APPENDIX B
THE EFFECTS OF TIME DELAYS

Let us assume that primary frequency controllers are affected by time delay in their actuators and/or measurement and these can be approximated by a first-order system as suggested in [39]. In this case, the average model of an ac power system can be modeled by the following cascade system:

$$\Sigma_0 : (\widetilde{x} + 1) M\dot{\widetilde{x}} = -D_L\widetilde{x}(\widetilde{x} + 1) + u - w + (\widetilde{x} + 1)\sum_i y_i$$

$$\Sigma_i : \epsilon_i\dot{y_i} = -y_i - D_i\widetilde{x}$$

where D_L is the load damping [pu], $i = 1, \dots, n$, and y_i, ϵ_i, D_i are the active power output [pu], time delay [s] and frequency droop [pu] of the i-th primary frequency controller. All other variables are as defined in Section II.

The admissible equilibrium set of the cascade system is

$$\mathcal{E} \triangleq \left\{ X \in \mathbb{R}^{(n+1)} \mid \dot{X} = 0 \right\}, X = \begin{bmatrix} \widetilde{x} & y_1 & \cdots & y_n \end{bmatrix}^\top$$

In the equilibrium (i.e. $\dot{y_i} = 0$), the output of primary frequency controllers is $y_i = -D_i\widetilde{x}$. As consequence, the equilibrium analysis of the complete system is reduced to solving in $x^\star, u^\star, w^\star$ the following equation:

$$0 = u^\star - w^\star - (x^\star + 1)x^\star \left(D_L + \sum_i D_i \right)$$

which produces the same results from Appendix A when considering $D = D_L + \sum_i D_i$. In conclusion, the equilibrium around $x^\star = 0$ is independent of the time delays ϵ_i and affected only by the total system damping D and the active power imbalance $u^\star - w^\star$. By induction, it is also possible to realize that time delays modeled by higher-order functions such as those presented in [40] will render the same results.

On the other hand, time delays may affect the stability of the cascade system. Let us consider:

$$\mathcal{V}(X) = \frac{1}{2}X^\top \begin{bmatrix} M & 0 & \cdots & 0 \\ 0 & \epsilon_1 & \cdots & 0 \\ \vdots & \vdots & \ddots & \vdots \\ 0 & 0 & \cdots & \epsilon_n \end{bmatrix} X$$

as a Lyapunov function candidate. Its time derivative for the unperturbed system (i.e. $u - w = 0$) is given by:

$$\dot{\mathcal{V}} = - \begin{bmatrix} M\widetilde{x} \\ \epsilon_1 y_1 \\ \vdots \\ \epsilon_n y_n \end{bmatrix}^\top \underbrace{\begin{bmatrix} \frac{D_L}{M} & -\frac{1}{\epsilon_1} & \cdots & -\frac{1}{\epsilon_n} \\ \frac{D_1}{M} & \frac{1}{\epsilon_1} & \cdots & 0 \\ \vdots & \vdots & \ddots & \vdots \\ \frac{D_n}{M} & 0 & \cdots & \frac{1}{\epsilon_n} \end{bmatrix}}_{Q} \begin{bmatrix} M\widetilde{x} \\ \epsilon_1 y_1 \\ \vdots \\ \epsilon_n y_n \end{bmatrix}$$

Note that $\dot{\mathcal{V}}$ is a quadratic form, hence $\dot{\mathcal{V}} < 0 \iff Q > 0$, which is indeed the condition for exponential stability of the cascade system. Using the argument that $Q_{sym} = \frac{1}{2}(Q + Q^\top)$ and Kron reduction, it is possible to show that the cascade system is stable if and only if $\epsilon_{max} < \frac{M}{D}$.

However, a proper stability analysis must also consider local and inter-area active power oscillations and rotor angle stability, which is assumed as pre-requisite here. This demands a proper distribution of damping and inertia among primary frequency controllers. An extensive discussion about this topic is found in [36].

APPENDIX C
INPUT-TO-STATE STABILITY THEOREM

Theorem 1: 4.19 in [27] Let $\mathcal{V} : [0, \infty) \times \mathbb{R}^n \to \mathbb{R}$ be a continuously differentiable function such that

$$\alpha_1(\|x\|) \leq \mathcal{V}(t, x) \leq \alpha_2(\|x\|)$$

$$\frac{\delta \mathcal{V}}{\delta t} + \frac{\delta \mathcal{V}}{\delta x} f(t, x, u) \leq -W_3(x), \ \forall \|x\| \geq \rho(\|u\|) > 0$$

$\forall (t, x, u) \in [0, \infty) \times \mathbb{R}^n \times \mathbb{R}^m$, where α_1, α_2 are class $\mathcal{K}_\infty$ functions, ρ is a class $\mathcal{K}$ function, and $W_3(x)$ is a continuous positive definite function on $\mathbb{R}^n$. Then, the system

$$\dot{x} = f(t, x, u)$$

is input-to-state stable with $\gamma = \alpha_1^{-1} \circ \alpha_2 \circ \rho$, where $f : [0, \infty) \times \mathbb{R}^n \times \mathbb{R}^m \to \mathbb{R}^n$ is piecewise continuous in t and locally Lipschitz in x and u, and the input $u(t)$ is a piecewise continuous, bounded function of t for all $t \geq 0$.

ACKNOWLEDGMENT

REFERENCES

[1] H. Farhangi, "The path of the smart grid," *IEEE Power Energy Mag.*, vol. 8, no. 1, pp. 18–28, Jan. 2010.

[2] G. Strbac, N. Hatziargyriou, J. P. Lopes, C. Moreira, A. Dimeas, and D. Papadaskalopoulos, "Microgrids: Enhancing the resilience of the European megagrid," *IEEE Power Energy Mag.*, vol. 13, no. 3, pp. 35–43, May 2015.

[3] D. Lew *et al.*, "Secrets of successful integration: Operating experience with high levels of variable, inverter-based generation," *IEEE Power Energy Mag.*, vol. 17, no. 6, pp. 24–34, Nov. 2019.

[4] J. Matevosyan *et al.*, "Grid-forming inverters: Are they the key for high renewable penetration?," *IEEE Power Energy Mag.*, vol. 17, no. 6, pp. 89–98, Nov. 2019.

[5] F. Milano, F. Dorfler, G. Hug, D. J. Hill, and G. Verbic, "Foundations and challenges of low-inertia systems," in *Proc. IEEE, Power Syst. Comput. Conf.*, Dublin, Jun. 2018, pp. 1–25.

[6] S. Y. Caliskan and P. Tabuada, "Uses and abuses of the swing equation model," in *Proc. 54th IEEE Conf. Decis., Control*, Osaka, Dec. 2015, pp. 6662–6667.

[7] *IEEE Standard for Interconnection and Interoperability Distributed Energy Resources with Associated Electric Power Syst. Interfaces*, IEEE 1547-2018, New York, NY, USA, 2018.

[8] *IEEE Standard for Testing Microgrid Controllers*. New York, IEEE 2030.8-2018, NY, USA, 2018.

[9] J. Schiffer, D. Zonetti, R. Ortega, A. M. Stanković, T. Sezi, and J. Raisch, "A survey on modeling of microgrids—From fundamental physics to phasors and voltage sources," *Autom.*, vol. 74, pp. 135–150, Dec. 2016.

[10] A. Bidram and A. Davoudi, "Hierarchical structure of microgrids control system," *IEEE Trans. Smart Grid*, vol. 3, no. 4, pp. 1963–1976, Dec. 2012.

[11] E. Rokrok, M. Shafie-khah, and J. P. Catalão, "Review of primary voltage and frequency control methods for inverter-based islanded microgrids with distributed generation," *Renew. Sustain. Energy Rev.*, vol. 82, pp. 3225–3235, Feb. 2018.

[12] P. P. Varaiya, F. F. Wu, and J. W. Bialek, "Smart operation of smart grid: risk-limiting dispatch," *Proc. IEEE*, vol. 99, no. 1, pp. 40–57, Jan. 2011.

[13] J. Laghari, H. Mokhlis, A. Bakar, and H. Mohamad, "Application of computational intelligence techniques for load shedding in power systems: A review," *Energy Convers. Manag.*, vol. 75, pp. 130–140, Nov. 2013.

[14] C. Gamarra and J. M. Guerrero, "Computational optimization techniques applied to microgrids planning: A review," *Renew. Sustain. Energy Rev.*, vol. 48, pp. 413–424, Aug. 2015.

[15] M. A. Al-Jaafreh and G. Mokryani, "Planning and operation of LV distribution networks: A comprehensive review," *IET Energy Syst. Integ.*, vol. 1, no. 3, pp. 133–146, Sep. 2019.

[16] P. Mercier, R. Cherkaoui, and A. Oudalov, "Optimizing a battery energy storage system for frequency control application in an isolated power system," *IEEE Trans. Power Syst.*, vol. 24, no. 3, pp. 1469–1477, Aug. 2009.

[17] G. Delille, B. Francois, and G. Malarange, "Dynamic frequency control support by energy storage to reduce the impact of wind and solar generation on isolated power system's inertia," *IEEE Trans. Sustain. Energy*, vol. 3, no. 4, pp. 931–939, Oct. 2012.

[18] L. Sigrist, I. Egido, E. Lobato Miguelez, and L. Rouco, "Sizing and controller setting of ultracapacitors for frequency stability enhancement of small isolated power systems," *IEEE Trans. Power Syst.*, vol. 30, no. 4, pp. 2130–2138, Jul. 2015.

[19] I. Egido, L. Sigrist, E. Lobato, L. Rouco, and A. Barrado, "An ultracapacitor for frequency stability enhancement in small-isolated power systems: Models, simulation and field tests," *Appl. Energy*, vol. 137, pp. 670–676, Jan. 2015.

[20] G. W. Chang, C.-S. Chuang, T.-K. Lu, and C.-C. Wu, "Frequency-regulating reserve constrained unit commitment for an isolated power system," *IEEE Trans. Power Syst.*, vol. 28, no. 2, pp. 578–586, May 2013.

[21] Y. Wen, W. Li, G. Huang, and X. Liu, "Frequency dynamics constrained unit commitment with battery energy storage," *IEEE Trans. Power Syst.*, vol. 31, no. 6, pp. 5115–5125, Nov. 2016.

[22] S. Abhyankar, G. Geng, M. Anitescu, X. Wang, and V. Dinavahi, "Solution techniques for transient stability-constrained optimal power flow – Part I," *IET Gener. Transmiss. Distrib.*, vol. 11, no. 12, pp. 3177–3185, Aug. 2017.

[23] G. Geng, S. Abhyankar, X. Wang, and V. Dinavahi, "Solution techniques for transient stability-constrained optimal power flow – Part II," *IET Gener. Transmiss., Distrib.*, vol. 11, no. 12, pp. 3186–3193, Aug. 2017.

[24] N. Nguyen, S. Almasabi, A. Bera, and J. Mitra, "Optimal power flow incorporating frequency security constraint," *IEEE Trans. Ind. Appl.*, vol. 55, no. 6, pp. 6508–6516, Nov. 2019.

[25] *IEEE PES Task Force on Benchmark Systems for Stability Controls, "Benchmark Systems for Small-Signal Analysis and Control,"* New York, NY, USA, Tech. Rep. PES-TR18, Aug. 2015.

[26] C. Tavora and O. M. Smith, "Characterization of equilibrium and stability in power systems," *IEEE Trans. Power App. Syst.*, vol. PAS-91, no. 3, pp. 1127–1130, May 1972.

[27] H. K. Khalil, *Nonlinear System*, 3rd ed. Upper Saddle River, NJ: Prentice Hall, 2002.

[28] P. Kundur, N. J. Balu, and M. G. Lauby, *Power System Stability and Control*, The EPRI Power System Engineering. New York: McGraw-Hill, 1994.

[29] J. Machowski, J. W. Bialek, and J. R. Bumby, *Power System Dynamics: Stability and Control*, 2nd ed. Chichester, U.K.: Wiley, 2008.

[30] E. F. Alves, "efantnu/ips-freq-stability: Data set and simulation files As submitted after Review 1 in IEEE TPWRS (Version 1.1)," Zenodo, Nov. 2, 2020, doi: 10.5281/zenodo.4192157.

[31] Comission Regulation (EU), "EU 2017/1485 guideline on electricity transmission system operation," Aug. 2017. [Online]. Available: https://eur-lex.europa.eu/eli/reg/2017/1485/oj

[32] J. W. Simpson-Porco, F. Dörfler, and F. Bullo, "Synchronization and power sharing for droop-controlled inverters in islanded microgrids," *Automatica*, vol. 49, no. 9, pp. 2603–2611, Sep. 2013.

[33] L. O. Nord, "Innovative Hybrid energy system for stable power and heat supply in offshore oil & gas installation (HES-OFF)," Jun. 2018. Accessed: Jun. 29, 2020. [Online]. Available: http://www.ntnu.edu/ept/hes-off/

[34] L. Riboldi and L. Nord, "Offshore power plants integrating a wind farm: Design optimisation and techno-economic assessment based on surrogate modelling," *Processes*, vol. 6, no. 12, p. 249, Dec. 2018.

[35] L. Riboldi, E. F. Alves, M. Pilarczyk, E. Tedeschi, and L. O. Nord, "Innovative hybrid energy system for stable power and heat supply in offshore oil & gas installation (HES-OFF): System design and grid stability," in *Proc. 30th Eur. Symp. Comput. Aided Process. Eng.*, vol. A. Milano, Italy: Elsevier, May 2020, pp. 211–216.

[36] F. Dörfler and F. Bullo, "Synchronization and transient stability in power networks and nonuniform Kuramoto oscillators," *SIAM J. Control Optim.*, vol. 50, no. 3, pp. 1616–1642, Jan. 2012.

[37] N. Modig *et al.*, "Technical Requirements for fast frequency reserve provision in the nordic synchronous area," ENTSO-E, Brussels, Belgium, Tech. Rep., 5 2019.

[38] ENTSO-E, "Fast Frequency Reserve – Solution to the Nordic inertia challenge," ENTSO-E, Brussels, Belgium, Tech. Rep., Dec. 2019. [Online]. Available: https://www.epressi.com/media/userfiles/107305/1576157646/fast-frequency-reserve-solution-to-the-nordic-inertia-challenge-1.pdf

[39] I. Egido, F. Fernandez-Bernal, P. Centeno, and L. Rouco, "Maximum frequency deviation calculation in small isolated power systems," *IEEE Trans. Power Syst.*, vol. 24, no. 4, pp. 1731–1738, Nov. 2009.

[40] IEEE Task Force on Turbine-Governor Modeling, "Dynamic models for turbine-governors in power system studies," IEEE, New York, NY, Tech. Rep. PES-TR1, 2013. [Online]. Available: https://resourcecenter.ieee-pes.org/publications/technical-reports/PESTR1.html

Danilo Brandao (Member, IEEE) received the Ph.D. degree in electrical engineering from the University of Campinas, Campinas, Brazil, in 2015. He was a Visiting Scholar with the Colorado School of Mines, USA, in 2009 and 2013, also with the University of Padova, Italy, in 2014, and a Guest Professor with the Norwegian University of Science and Technology, Norway, in 2018 and 2020. He is currently an Assistant Professor with the Graduate Program in electrical engineering with the Federal University of Minas Gerais, Belo Horizonte, Brazil. His main research interests are control of grid-tied converters and microgrids. Dr. Brandao is a member of SOBRAEP.

Erick Alves (Senior Member, IEEE) received the engineering degree in energy and automation from the University of São Paulo, São Paulo, Brazil, in 2007, and the M.Sc. degree in electrical engineering from the Arctic University of Norway, Narvik, Norway, in 2018. He is currently working toward the Ph.D. degree with the Department of Electric Power Engineering, Norwegian University of Science and Technology, Trondheim, Norway focusing on power quality and stability of low-inertia ac grids. From 2007 to 2018, he held several positions with the Voith Group in Brazil, Norway, and Germany. During this period, he was involved in the design, engineering, commissioning, and development of control systems for more 40 power plants in 18 countries. His latest assignment was with Voith Digital Ventures, Heidenheim, Germany, as Product Manager for power generation controls.

Elisabetta Tedeschi (Senior Member, IEEE) received the M.Sc. degree (Hons.) in electrical engineering and the Ph.D. degree in industrial engineering from the University of Padova, Padova, Italy, in 2005 and 2009, respectively, researching on cooperative control of compensation systems. From 2009 to 2011, she was a Postdoctoral Fellow with the Norwegian University of Science and Technology (NTNU), Trondheim, Norway researching on the design and control of energy conversion systems for the grid integration of offshore renewable energies. She was a Researcher with Tecnalia, Bilbao, Spain, from 2011 to 2013, where she worked on storage solutions for the grid integration of wave energy converters. From 2013 to 2014, she was a Research Scientist with SINTEF Energy, Trondheim, Norway and an Adjunct Associate Professor with NTNU, where she became a Full Professor within offshore grids in 2014. She has a core competence in the design and control of energy conversion and transmission systems, with focus on offshore energy and power-quality issues. She has led and/or contributed to more than 15 national and international scientific projects. She was a recipient of the Marie Curie Fellowship.

Gilbert Bergna-Diaz (Member, IEEE) received the electrical power engineering degree from the Universidad Simón Bolívar, Caracas, Venezuela, in 2008, the research master's degree in electrical energy from the École Supérieure dÉlectricité (Supélec), Paris, France, in 2010, and the joint Ph.D. degree in electric power engineering from École Centrale Supélec, Paris, and the Norwegian University of Science and Technology (NTNU), Trondheim, Norway, in 2015. In 2014, he joined SINTEF Energy Research as a Research Scientist, where he was involved in modelling, analysis, and control of HVdc transmission systems. In 2016, he joined the Department of Electric Power Engineering with NTNU as a Postdoctoral Research Fellow, where he was involved in energy-based modeling and nonlinear control of multiterminal HVdc grids and, since 2019, he serves as an Associate Professor with the same department.